Quantifying phonon-induced non-Markovianity in color centers in diamond

Ariel Norambuena, Jerónimo R. Maze, Peter Rabl, and Raúl Coto

Phys. Rev. A **101**, 022110 — Published 20 February 2020

DOI: 10.1103/PhysRevA.101.022110

Quantifying phonon-induced non-Markovianity in color centers in diamond

Ariel Norambuena,[1,2,*] Jerónimo R. Maze,[3] Peter Rabl,[4] and Raúl Coto[1,†]

[1] *DAiTA Lab, Facultad de Estudios Interdisciplinarios, Universidad Mayor, Chile*
[2] *Centro de Óptica e Información Cuántica, Facultad de Ciencias, Universidad Mayor, Chile*
[3] *Instituto de Física, Pontificia Universidad Católica de Chile, Casilla 306, Santiago, Chile*
[4] *Vienna Center for Quantum Science and Technology, Atominstitut, TU Wien, 1040 Vienna, Austria*

(Dated: January 27, 2020)

We propose the application of a coherence-based measure for non-Markovianity to study the dynamics of color centers in diamond, where the optical coherence between two orbital states is affected by interactions with a structured phonon bath. Although limited to pure dephasing, we show that this measure is well-behaved at arbitrary temperatures and experimentally accessible through Ramsey spectroscopy. By taking realistic phonon spectral density functions into account, we use this quantity to show how non-Markovianity is affected by the presence of both bulk and quasi-localized phonon modes, as relevant for most defects in solids. Importantly, with only a minor modification the measure can be adapted to study the source of non-Markovianity in driven two-level systems and is thus applicable for a large class of systems modeled by the spin-boson Hamiltonian.

I. INTRODUCTION

By employing the principles of superposition and entanglement, quantum systems can outperform their classical counterparts in many applications such as computation, cryptography and high-precision measurements [1–3]. However, to benefit from this quantum advantage, the systems must be protected from detrimental interactions with the environment using passive isolation as well as active techniques such as error correction or decoupling pulses. To implement efficient error-mitigation schemes it is crucial to have a precise understanding of the underlying system-environment interaction [4], in particular in realistic non-Markovian settings, where information can flow back from the bath to the system and is not immediately lost. These scenarios have been exploited, for example, for quantum metrology [5], quantum channels [6], entangling protocols [7] or quantum control [8] and led to a growing interest in the questions how different environments can be compared and how non-Markovianity (NM) can be quantified [9–12].

While a variety of completely general measures for NM have already been proposed, those measures involve, for example, the maximization of the trace distance between two different initial states [9], the addition of auxiliary systems [10] or the complete knowledge of the dynamical map [11]. This makes proof-of-concept demonstrations and the broad use of such measures for modeling realistic applications very cumbersome. However, in many situations of interest the effect of the environment is naturally constraint to pure dephasing, in which case a measure for NM can be directly derived from the coherence of the system [13, 14]. This quantity is most essential for quantum technology applications and in many cases it can be directly accessed through Ramsey measurements. It is thus important to analyze such measures for NM not only from a mathematical point of view, but also to study their behavior in realistic settings.

In this paper we introduce and investigate a coherence-based measure suitable for characterizing NM features in the dephasing dynamics of color centers in solids. Specifically, we focus on the silicon-vacancy (SiV^-) and nitrogen-vacancy (NV^-) centers in diamond, which have attracted wide attention because the quantum state of these centers can be initialized, controlled and read out with high fidelity [15–17]. These unique properties make them strong candidates for various quantum sensing and quantum information processing application [18, 19], but their optical properties are still limited by unavoidable interactions with phonons. The influence of a continuum of bulk modes and distinct quasi-localized resonances originates a rich and complex dynamics arising from different NM behavior beyond the extensively studied Ohmic environment [20]. Based on this real-world example, we show that our considered measure for NM is well-behaved and physically meaningful at arbitrary temperatures, and can thus be used to obtain a deeper understanding of the NM dynamics also in more general phononic baths. This can be important for engineering and optimizing defect-phonon interactions in structured reservoirs such as cantilevers [21], two-dimensional layers [22], phonon waveguides [23] or phononic crystals [24, 25].

II. MEASURES OF NON-MARKOVIANITY

The dynamics of an open quantum system can be expressed in terms of a time-local master equation for the density operator ρ [31]

$$\dot{\rho}(t) = -\frac{i}{\hbar}[H(t),\rho(t)] + \sum_j \gamma_j^c(t)\left(L_j(t)\rho(t)L_j^\dagger(t) - \frac{1}{2}\{L_j^\dagger(t)L_j(t),\rho(t)\}\right), \quad (1)$$

where $H(t)$ is Hermitian and the L_j are a set of orthogonal jump operators $\mathrm{Tr}\{L_i^\dagger(t)L_j(t)\} = \delta_{ij}$. For a Markovian

* ariel.norambuena@umayor.cl
† raul.coto@umayor.cl

dynamics the canonical decay rates $\gamma_j^c(t)$ are positive and usually they are also constant in time, in general this is not necessarily the case. Therefore, assuming a single decay channel for simplicity, one can introduce the function $f(t) \equiv \max\{-\gamma^c(t), 0\} = (|\gamma^c(t)| - \gamma^c(t))/2$ [31] and define a measure for NM by integrating this function over a bound time interval, [11, 31],

$$\mathcal{N}_\gamma = \frac{1}{2}\int_t^{t'} \left(|\gamma^c(\tau)| - \gamma^c(\tau)\right)\, d\tau. \tag{2}$$

Note that this measure is related to the Rivas-Huelga-Plenio (RHP) measure by $\mathcal{N}_\gamma = (d_H/2)\mathcal{N}_{RHP}$ [11], where d_H is the dimension of the Hilbert space. In this approach, NM is witnessed from the negative values of $\gamma^c(t)$ [9–11, 32, 33].

In this work we follow another natural approach towards witnessing NM through the examination of the back-flow of quantum information in terms of the Coherence [26, 27]. For a given complete set of basis states $\{|i\rangle\}$, Coherence is commonly defined as $C(t) = \sum_{i\neq j} |\rho_{ij}(t)|$ [28], where the $\rho_{ij}(t) = \langle i|\rho(t)|j\rangle$ are the matrix elements of the system density operator. Although this definition is not unique, the choice of basis states usually follows naturally from the context and is very often taken as the eigenbasis of the bare system. For a two-level system the definition above reduces to $C(t) = \sqrt{\langle\sigma_x\rangle^2 + \langle\sigma_y\rangle^2}$, where the σ_k are the usual Pauli operators. In this case, $C(t)$ can be experimentally attained through standard Ramsey spectroscopy, *i.e.*, by applying two $\pi/2$-pulses separated by a time t. A measurement of the final population in the excited state, $P_e = (1 + \langle\sigma_x\rangle)/2$, then provides a measurement of $\langle\sigma_x\rangle$, or $\langle\sigma_y\rangle$, if an additional rotation between the two pulses is introduced. Similar strategies can also be applied to measure $C(t)$ for higher dimensional systems, where, however, the pulse sequences are slightly more involved.

Coherence does not increase under incoherent completely positive and trace preserving (ICPTP) maps [28], *i.e.*, $dC/dt \leq 0$. Hence, for a pure dephasing decay channel (transverse relaxation)[29], it can be used to detect non-Markovianity given a violation of this monotonicity $dC/dt > 0$. We use the following measure for such incoherent open system dynamics

$$\mathcal{N}_C = \max_{\rho(0)\in\mathcal{I}^c} \int_{dC(\rho(t))/dt>0} \frac{dC(\rho(t))}{dt}\, dt, \tag{3}$$

where the maximization takes into account initial states $\rho(0)$ belonging to the set of coherent states $\mathcal{I}^c$. Even though $\mathcal{N}_C$ might be considered as a basis-dependent measure, a quantum resource theory support its applicability regardless of such dependency [30].

III. OPTICAL COHERENCE FOR ORBITAL STATES OF COLOR CENTERS

In this section, we investigate in more detail the application of the above defined measures $\mathcal{N}_C$ and $\mathcal{N}_\gamma$ for SiV^- and NV^- centers in diamond. In the frame rotating with the frequency ω_L of a driving laser, the Hamiltonian reads ($\hbar = 1$) [34, 35]

$$H = \frac{\Delta}{2}\sigma_z + \frac{\Omega}{2}\sigma_x + \sum_k \omega_k a_k^\dagger a_k + \frac{\sigma_z}{2}\sum_k g_k\left(a_k + a_k^\dagger\right), \tag{4}$$

where $\Delta = \omega_{eg} - \omega_L$ is the detuning from the bare transition frequency ω_{eg} and Ω is the optical Rabi frequency. The $g_k = \lambda_{e,k} - \lambda_{g,k}$ [36] denote the effective electron-phonon coupling constants, which arise from the different deformation potentials, $\lambda_{e,k}$ and $\lambda_{g,k}$, in the ground and the excited state.

During the free evolution time ($\Omega = 0$) we assume that the phonon reservoir is initially in a thermal state $\rho_{ph} = \exp(-\beta H_{ph})/\mathrm{Tr}\{e^{-\beta H_{ph}}\}$, where $\beta = (k_B T)^{-1}$ and $H_{ph} = \sum_k \omega_k a_k^\dagger a_k$. The exact orbital dynamics of the color center is described by the following time-local master equation in the interaction picture [32, 37]

$$\frac{d\rho_s}{dt} = -\frac{\gamma(t)}{2}(\rho_s(t) - \sigma_z\rho_s(t)\sigma_z). \tag{5}$$

The system-environment interaction is fully determined by the time-dependent dephasing rate [37] ($\hbar = 1$)

$$\gamma(t) = \int_0^\infty \frac{J(\omega)}{\omega}\coth\left(\frac{\omega}{2k_BT}\right)\sin(\omega t)\, d\omega, \tag{6}$$

where $J(\omega) = \sum_k |g_k|^2\delta(\omega - \omega_k)$ is the spectral density function (SDF), k_B is the Boltzmann constant and T is the reservoir temperature. In general, the SDF satisfies two important properties: i) $J(0) = J(\omega > \omega_{max}) = 0$ and ii) $J(\omega) > 0\ \forall\ \omega \in (0, \omega_{max})$, where ω_{max} is the largest phonon frequency of the reservoir. The formal solution of the off-diagonal elements of $\rho_s(t)$ is given by $\rho_{eg}(t) = \rho_{eg}(0)e^{-\Gamma(t)}$, where $\Gamma(t) = \int_0^t \gamma(\tau)\, d\tau$ is a bounded function that satisfies $0 \leq \Gamma(t) \leq 2\int_0^\infty J(\omega)/\omega^2\mathrm{coth}(\omega/2k_BT)\, d\omega$. Furthermore, for this particular case the coherence is given by

$$C(t) = 2|\rho_{eg}(0)|e^{-\Gamma(t)}, \tag{7}$$

where $\rho_{eg}(0) = \langle e|\rho(0)|g\rangle$ is the initial condition for the off-diagonal element. As a result, $\mathcal{N}_C$ can be found as [13]

$$\mathcal{N}_C = -2\int_{\gamma(t)<0} \gamma(t)e^{-\Gamma(t)}\, dt. \tag{8}$$

Note that the non-Markovian behavior is intrinsically related with the back-flow of quantum information, *i.e.*, when $\gamma(t) < 0$. For this particular case, where the effect of the environment represented in Eq. (5) only induces a pure dephasing dynamics, the orthonormality is fulfilled by $\mathrm{Tr}\{L_z^\dagger L_z\} = 1$ [11, 31] ($L_z = \sigma_z/\sqrt{2}$), and thus $\gamma^c(t) = \gamma(t)$. In the next section, we introduce the phononic spectral density function in order to study the effect of phonons in a realistic diamond lattice.

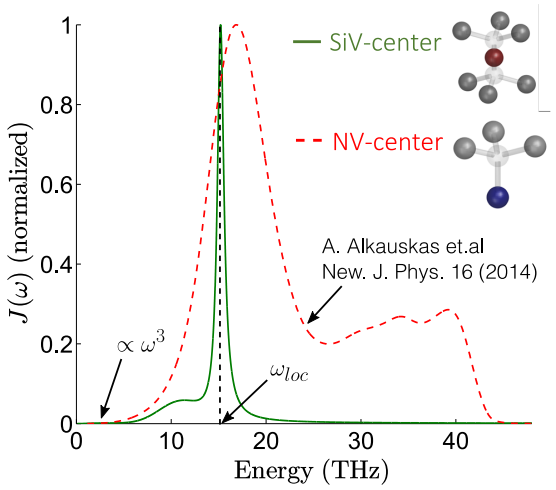

FIG. 1. (Color online) Spectral density function of the SiV^- and NV^- centers. Green (solid) and red (dashed) curves correspond to the phenomenological model $J(\omega) = J_{bulk}(\omega) + J_{loc1}(\omega) + J_{loc2}(\omega)$ given in Eqs. (9)-(11) and the first-principles spectral density function calculated in Ref. [41], respectively. At low frequencies, both curves have a dominant contribution of acoustic phonons leading to $J(\omega) \propto \omega^3$. The main peak of the green curve (SiV^-) is the contribution of a quasi-localized phonon mode with frequency $\omega_{loc} \approx 15.19$ THz.

IV. PHONON SPECTRAL DENSITY AND DEPHASING RATE

From Eq. (6) we see that the dephasing rate $\gamma(t)$, and thus the degree of NM, depends only on the SDF, $J(\omega)$, and the temperature T. In the case of color centers or other solid-state emitters, information about the SDF can be obtained from the photoluminescence (PL) spectrum [36, 38], where the coupling to the phonons both reduces the bare resonance (zero-phonon line) and leads to additional phonon-sidebands. The experimental PL spectrum of the SiV^- center exibits an isotopic shift feature in the prominent and narrow phonon sideband [38]. This can be explained by the strong electron-phonon interaction with a quasi-localized phonon mode primarily composed of a large oscillation of the silicon atom [36, 38, 39]. In addition, lattice vibrations in the bulk lead to a smooth SDF, which typically scales as $\sim \omega^3$ for low frequencies in a three-dimensional lattice. The phononic SDF that reproduces the isotopic shift feature of the PL spectrum and the effect of acoustic phonons is phenomenologically given by $J(\omega) = J_{bulk}(\omega) + J_{loc1}(\omega) + J_{loc2}(\omega)$, with [36]

$$J_{bulk}(\omega) = 2\alpha\omega_c^{1-d}\omega^d e^{-\omega/\omega_c}, \tag{9}$$

$$J_{loc1}(\omega) = \frac{J_0\omega^d}{\left(\frac{\omega}{\omega_{loc}}+1\right)^2}\frac{\Gamma/2}{(\omega-\omega_{loc})^2+(\Gamma/2)^2}, \tag{10}$$

$$J_{loc2}(\omega) = J_1\omega^d e^{-(\omega-\omega_0)^2/(2\sigma^2)}, \tag{11}$$

where d is the dimension of the diamond lattice ($d = 3$ in our case). Acoustic phonons are associated with low-energy vibrational excitations where the atoms of the color center are oscillating in phase and therefore experimenting a weak electron-phonon interaction. Thus, these phonons are reasonably well described by an intensity α and a cutoff frequency $\omega_c \simeq 1$ THz. However, quasi-localized phonon modes induce out-of-phase oscillations of the defect's atoms with large amplitude leading to a strong electron-phonon interaction. This type of interactions is usually modeled by Lorentzian-like functions centered around the specific localized phonon frequency ω_{loc}, with a characteristic width Γ and an intensity J_0. For the region in between (from 1 THz to ~14 THz) other vibrational modes participate [40], which is captured by the Gaussian contribution $J_{loc2}(\omega)$. For the SiV^- center, the following parameters of the SDF are chosen to accurately match the PL spectrum obtained from molecular dynamic simulations: $\alpha = 0.0275$, $J_1 = 0.0025$ THz^{-2}, $\sigma = 2.4042$ THz, $\omega_0 = 9.35$ THz, $J_0 = 0.0235$ THz^{-1}, $\Gamma = 0.8414$ THz, and $\omega_{loc} = 15.19$ THz. For the NV^- center we do not make this decomposition and use the exact SDF obtained from a detailed first-principles calculation reported in Ref. [41]. In Figure 1 we plotted the normalized spectral density functions of both NV^- and SiV^- centers.

By following the same partition as for the SDF, we write for the SiV^- center the total dephasing rate defined in Eq. (6) as $\gamma(t) = \gamma_{bulk}(t) + \gamma_{loc1}(t) + \gamma_{loc2}(t)$. In order to better illustrate the behavior of the individual contributions we will first consider the limit of very low temperatures where $\coth(\omega/2k_BT) \approx 1$ and

$$\gamma^{\downarrow}_{bulk}(t,d) = 2\alpha\omega_c(d-1)!\frac{\sin(d\tan^{-1}(\omega_c t))}{[1+(\omega_c t)^2]^{d/2}}, \tag{12}$$

$$\gamma^{\downarrow}_{loc1}(t) \approx \frac{1}{4}J_0\omega_{loc}^2\pi\sin(\omega_{loc}t)e^{-\Gamma t/2}, \tag{13}$$

$$\gamma^{\downarrow}_{loc2}(t) = J_1\int_0^\infty \omega^2 e^{-(\omega-\omega_0)^2/(2\sigma^2)}\sin(\omega t)\,d\omega. \tag{14}$$

For a detailed derivation of the dephasing rate $\gamma^{\downarrow}_{loc1}(t)$ see Appendix B. We left $\gamma^{\downarrow}_{loc2}(t)$ in terms of the integral since it involves a rather complicated expression. Note that Eq. (12) is only valid for $d > -1$, which is satisfied in our case ($d = 3$). In the opposite, high temperature regime, $\omega/2k_BT \ll 1$ and $\coth(\omega/2k_BT) \approx 2k_BT/\omega$. In this case we obtain $\gamma^{\uparrow}_{bulk}(t) = (2k_BT/\omega_c)\,\gamma^{\downarrow}_{bulk}(t,d-1)$, $\gamma^{\uparrow}_{loc1}(t) \approx (2k_BT/\omega_{loc})\,\gamma^{\downarrow}_{loc1}(t)$ and $\gamma^{\uparrow}_{loc2}(t) = 2k_BTJ_1\int_0^\infty \omega\exp(-(\omega-\omega_0)^2/(2\sigma^2))\sin(\omega t)\,d\omega$.

Figure 2 shows the expected dephasing rates for the SiV^- center in diamond for low and high temperatures. Moreover, based on numerical simulations we set the low (high) temperature regime to be below (above) $T \approx 20$ K (286 K). These boundaries have been chosen such that the approximate low- and high-temperature limits for the dephasing rate given above match its exact numerical shape. From the statistical properties of the phonon reservoir, in particular, the mean number of phonons $n(w) = [\exp(\hbar\omega/k_BT)-1]^{-1}$, we observe that $n(\omega_{loc}) \approx 2$ for $T \approx 286$ K and $\omega_{loc} = 15.19$ THz. In other words, the high-temperature regime is defined from the thermal activation of the strong electron-phonon coupling with the quasi-localized phonon mode.

If we individually look at the components of $\gamma(t)$, it is straightforward to notice that each one will get involved in the dynamics at a different temperature. For $\gamma_{bulk}(t)$ in Figure 2-(a) we observe a region where it takes negative values, and above a critical temperature ($T_c \approx 1.85$ K) it is always positive. However, $\gamma_{loc1}(t)$ and $\gamma_{loc2}(t)$ show negative values even at room temperature, with an amplitude that is non-negligible as compared to the low-temperature case, see Figures 2-(b) and 1-(c). This negative behavior has previously been connected to memory effects [10], as we will detail in what follows. Finally, one can notice that $\gamma_{loc1}(t)$ has the leading contribution to the dephasing rate, see Figure 2-(d). For comparison, in Appendix C we evaluate the dephasing rate for a NV^- center, which also exhibits negative values at room temperature. In a recent experiment with a NV^- center, ultrafast vibrational relaxation dynamics with a time constant around 50 fs was revealed [42], evidencing that the fast dynamics exhibits by the dephasing rates can be studied using spectrally resolved optical pump-probe spectroscopy. Moreover, another experiment uses the inherent nitrogen spin as a source for controllable non-Markovian dynamics [43], leading to a deep and practical understanding of its effect.

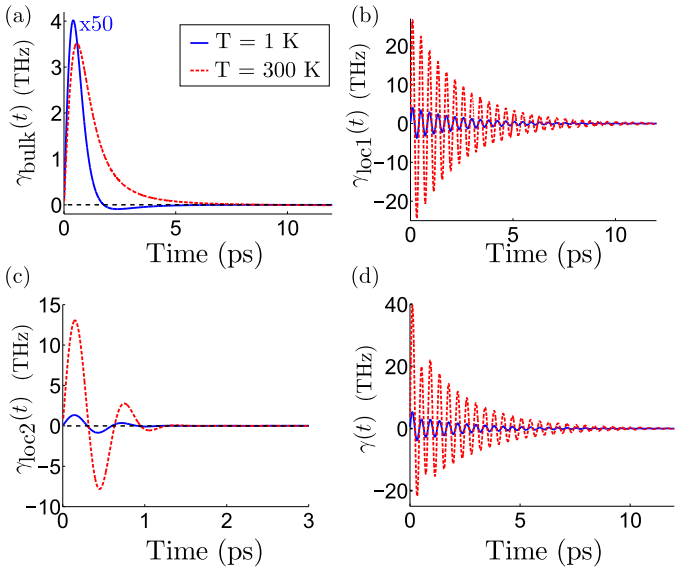

FIG. 2. The dephasing rate is plotted separately by considering each contribution of the phononic spectral density function: (a) $J_{bulk}(\omega)$ (acoustic phonons), (b) $J_{loc1}(\omega)$ (strong interaction with a quasi-localized phonon), (c) $J_{loc2}(\omega)$ (gaussian spectral function), and (d) the whole contribution given by $J(\omega) = J_{bulk}(\omega) + J_{loc1}(\omega) + J_{loc2}(\omega)$. Blue (solid) and red (dashed) curves shows temperature effects on the dephasing rate for $T = 1$ K and $T = 300$ K, respectively. In (b) and (d) the period of the oscillations are approximately given by $2\pi/\omega_{loc} \approx 0.41$ ps, where $\omega_{loc} = 15.19$ THz is the frequency associated with the strong electron-phonon coupling illustrated in Figure 1.

V. NON-MARKOVIANITY IN COLOR CENTERS AND THERMAL EFFECTS

Let us now discuss the degree of NM of the described phonon environment, as quantified through $\mathcal{N}_C$ and $\mathcal{N}_\gamma$. Firstly, the definition of $\mathcal{N}_\gamma$ in Eq. (2) and the relation $\gamma^c(t) = \gamma(t)$ implies that the previous discussion about the negative behavior of $\gamma(t)$ in Figure 2 stands as a proof of NM for the orbital states of the SiV^- center— similar conclusions are obtained for the NV^- center. This result is the first evidence that the phononic contribution induces NM behavior in color centers in diamond, commonly modeled as purely Markovian [21, 44, 45].

In Figure 3-(a) we show the temperature dependence of $\mathcal{N}_C$ (dashed lines) and $\mathcal{N}_\gamma$ (solid lines) for both color centers in diamond (NV^- and SiV^-). It is interesting that both measures are almost constant at low temperatures, but above $T \approx 100$ K, $\mathcal{N}_\gamma$ starts to increase linearly with temperature, while in contrast, $\mathcal{N}_C$ goes to zero. The former can be explained from the strong contribution of the quasi-localized phonon mode given by $\gamma_{loc1}(t) \approx (\pi J_0 \omega_{loc}^2/4)\coth(\omega_{loc}/2k_BT)\sin(\omega_{loc}t)e^{-\Gamma t/2}$ (see Appendix B), where $\coth(\omega_{loc}/2k_BT) = 2n(\omega_{loc}) + 1$ increases with temperature, being $n(\omega) = [\exp(\omega/k_BT) - 1]^{-1}$ the mean number of phonons at thermal equilibrium. Therefore, the criteria for NM based on the measure $\mathcal{N}_\gamma$ would lead to the conclusion that the bath becomes more NM with increasing temperature. In contrast, by looking at the time evolution of the Coherence plotted in Figure. 3(b), one immediately sees that the proposed quantity $\mathcal{N}_C$ in Eq. (3) disappears at high temperature, as one would expect from the coupling to bulk phonons. To shed more light on this matter, the key is to look at the unusual and complex spectral density function of these systems. On the one hand, at low temperatures the dynamics is determined by the SDF $J(\omega)$, since all phonons are frozen out. For this reason, the quasi-localized phonon has the leading contribution to NM, in agreement with the remarks given in Ref. [46] for an engineered reservoir. On the other hand, at high temperatures, low-frequency (acoustic) phonons are dominant ($\gamma^\uparrow(t) \sim \int_0^\infty J(\omega)/(\hbar\omega)^2 \sin\omega t\, d\omega$), and therefore the reservoir can be modeled by a super-Ohmic spectrum, see Appendix D. In this scenario, NM is highly suppressed [32].

It is worthwhile to point out that these two measures belong to different interpretations of NM, where $\mathcal{N}_\gamma$ is related to the divisibility of the evolution based on whether the canonical decay rates are positive or not [31], while $\mathcal{N}_C$ accounts for the back-flow of quantum information as the monotonicity of the Coherence breaks down. As a consequence, these two measures have opposite temperature responses as T increases. For instance, the dephasing rate comes from the interaction Hamiltonian $(1/2)\sigma_z \sum_k g_k(a_k + a_k^\dagger)$ which describe one-phonon processes. For this case, at high temperatures the amplitude of $\gamma(t)$ is proportional to T, that leads to $\mathcal{N}_\gamma \propto T$. On the contrary, the Coherence is connected with physical observables through the relation $C(t) = \sqrt{\langle\sigma_x\rangle^2 + \langle\sigma_y\rangle^2}$. Thus, the expectation values $\langle\sigma_i\rangle$ will depend on the matrix elements $\rho_{ij}(t) = \rho_{ij}(0)\exp(-2\int_0^t \gamma(\tau)\, d\tau)$, which at high

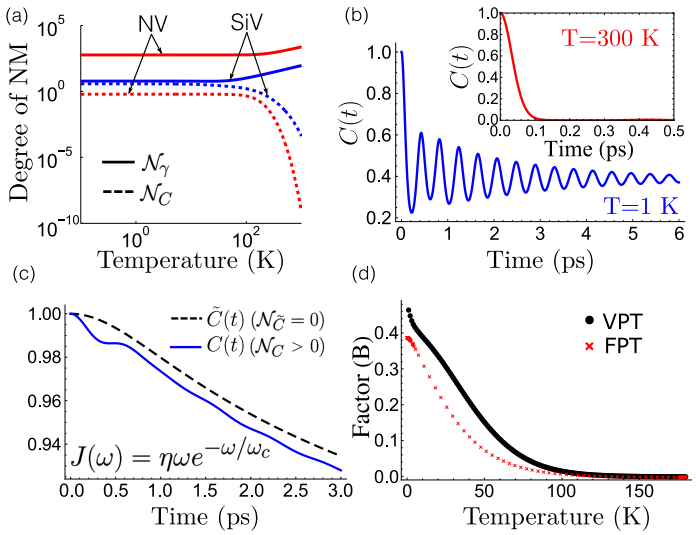

FIG. 3. (a) Comparison of the non-Markovian measures $\mathcal{N}_C$ and $\mathcal{N}_\gamma$ for the SiV$^-$ and NV$^-$ centers in logarithmic scale and for temperatures ranging from 10 mK to 300 K. For the SiV$^-$ center the SDF $J(\omega)=J_{bulk}(\omega)+J_{loc1}(\omega)+J_{loc2}(\omega)$ was used and for the NV$^-$ center the exact SDF given in Ref. [41]. The NM measure $\mathcal{N}_\gamma(T)=\int_t^{t'}(|\gamma(\tau)|-\gamma(\tau))\,d\tau$ was calculated using $t=0$ and a sufficient large time $t'=300$ ps. (b) Coherence function $C(t)$ reveals a back-flow of quantum information at low temperature while at room temperature it monotonically decreases. (c) Filtering function $S^{-1/2}$ allows to distinguish the origin of the NM for the generalized spin-boson model. We use the values $\eta=1$, $\omega_c=1$ THz, $T=0$ and $\Omega=4\Delta$, for a Ohmic spectral density function $J(\omega)$. (d) Renormalization factor B for the SiV$^-$ center using the full polaron transformation (FPT) and the variational polaron transformation (VPT) for $\Omega=0.6$ GHz and $\Delta=\Omega/2$.

temperatures leads to $\mathcal{N}_C\propto\exp(-\pi J_0 k_B T)$, as shown in Figure.3-(a). Henceforth, a comparison between these measures will contribute on the debate about how to use different criteria of NM for practical applications, such as modeling the vibrations of a diamond lattice at high temperatures [21, 44, 45, 47, 48], that can be simply considered as Markovian.

To further support the physical consistency of the coherence measure $\mathcal{N}_C$, we now compare it with the well-known measure proposed by Breuer, Laine, and Piilo ($\mathcal{N}_{BLP}$) [9], where the figure of merit is the trace distance between two quantum states, $D(t)=\mathrm{tr}|\rho_1-\rho_2|/2$, (see Appendix E for more details). Both measures have a similar behavior as a function of temperature, see Figure 6, although $\mathcal{N}_C$ can be easily computed and experimentally measured through a system observable such as $\langle\sigma_x\rangle$. Moreover, it does not involve an auxiliary system, in contrast to the case of quantum mutual information measure [10].

A. Coherent maps in the weak-coupling regime

In the current and many other settings of interest, the Rabi-frequency Ω in Hamiltonian (4) is controlled by an external drive and can be switched off. This scenario ($\Omega=0$) for pure dephasing channels has been extensively studied [32, 49]. However, this might not be the case for other systems, where a non-vanishing coupling ($\Omega\neq 0$) can induce oscillations between the states $|g\rangle$ and $|e\rangle$, and therefore induces oscillations in the Coherence. Since this dynamics lies outside the incoherent regime assumed in Eq. (3), it prevents the use of $\mathcal{N}_C$ as a strict measure for NM. However, we can still use it to distinguish whether the NM solely comes from the environment or from the environment plus the external laser. To do so, we propose here an experimental sequence for systems with a pure dephasing dynamics, which allows us to eliminate a possible NM signature from the term $(\Omega/2)\sigma_x$. This procedure allows us to study the phonon environment in terms of a simple measure of NM given by $\mathcal{N}_C$. We start from the master equation for $\rho_s(t)$ in Eq. (A1). The resulting time evolution for the off-diagonal elements is given by $\rho_{eg}(t)=\rho_{eg}(0)\exp(-i\omega_0 t-F_0(t)+F(t)/2)$, where $F_0(t)$ reduces to $\Gamma(t)$ for $\Omega=0$, with $\Gamma(t)=\int_0^t\gamma(\tau)\,d\tau$ and $\gamma(\tau)$ is given in Eq. (6). The function $F(t)$ contains contributions which are solely related to coherent population oscillations (see Appendix A), and therefore must be cancelled. This can be done by defining the following quantity [see Eq. (A12)],

$$S=\frac{1}{2}\left[\langle S_z\rangle|_{\rho(0)=|e\rangle\langle e|}-\langle S_z\rangle|_{\rho(0)=|g\rangle\langle g|}\right]=e^{F(t)},\qquad(15)$$

that depends on $F(t)$ only. Here the subscripts indicate that the average dynamics of $\langle S_z\rangle$ is calculated starting from the initial excited ($|e\rangle=|e_+\rangle$) and ground ($|g\rangle=|e_-\rangle$) eigenstates of the Hamiltonian $H_s=(\Delta/2)\sigma_z+(\Omega/2)\sigma_x$, with $|e_\pm\rangle=(\pm\Omega|e\rangle+(\omega_0\mp\Delta)|g\rangle)/\sqrt{2\omega_0(\omega_0\mp\Delta)}$ [50]. The operators S_i are the usual Pauli matrices written in the system eigenbasis. In summary, we implement the following three steps: (1) perform a measurement of $\langle S_z\rangle$ for the initial condition $\rho(0)=|g\rangle\langle g|$, (2) repeat the measurement for $\rho(0)=|e\rangle\langle e|$, (3) calculate the Coherence by performing a measurement of $\langle S_x\rangle$ and $\langle S_y\rangle$ for the initial pure state $|\varphi(0)\rangle=(|e\rangle+|g\rangle)/\sqrt{2}$, and multiply the outcome $C(t)=\sqrt{\langle S_x\rangle+\langle S_y\rangle}$ by $S^{-1/2}$. From this procedure we define a renormalized coherence $\tilde{C}(t)=C(t)\times S^{-1/2}$ which can be used instead of $C(t)$ in Eq. (3). Note that this sequence is unbiased with the spectral density function and it takes advantage of the dynamics induced by the σ_x component.

One remaining question is whether a violation of the monotonicity of $\tilde{C}(t)$, say $d\tilde{C}(t)/dt>0$, unavoidable leads to a non-Markovian signature for the reduced dynamics (applying the filter), as it was detailed for $C(t)$ in the absence of an external field ($\Omega=0$) in Section II. To begin, we note that from the definition of $\tilde{C}(t)$ it follows that

$$\tilde{C}(t)=C(t)\times S^{-1/2}=2|\rho_{eg}(0)|e^{-(\Delta/\omega_0)^2\Gamma(t)},\qquad(16)$$

with $\omega_0=\sqrt{\Delta^2+\Omega^2}$. By taking the time derivative on the above equation, we find that the condition for breaking the monotonicity of the function $\tilde{C}(t)$ is given by the sign of $d\Gamma(t)/dt$, that matches the one obtained for the incoherent

case $\Omega = 0$, see Eq. (7). Therefore, we conclude that the function $\tilde{C}(t)$ is a monotonically decreasing function in time if the reduced dynamics is Markovian, *i.e.* $d\tilde{C}(t)/dt \leq 0$. Correspondingly, it is non-Markovian when $d\tilde{C}(t)/dt > 0$.

For further illustration we consider the Ohmic SDF $J(\omega) = \eta\omega \exp(-\omega/\omega_c)$. We found that for $\Omega \neq 0$ the BLP measure in Eq. (E1) reveals a NM behavior. Now, we can distinguish where the NM comes from using the renormalized coherence $\tilde{C}(t)$ to define a NM measure $\mathcal{N}_{\tilde{C}}$ for the reduced dynamics. In Fig. 3-(c) we plot the coherence calculated with and without the filtering function $S^{-1/2}$. On the one hand, one can observe that, in agreement with the BLP measure, $\mathcal{N}_C$ detects NM. On the other hand, $\mathcal{N}_{\tilde{C}} = 0$ for the reduced dynamics. This means that the NM originates from the presence of the external laser and not from the reservoir alone. This conclusions is also supported by previous results with this SDF, where for $\Omega = 0$ and at arbitrary temperatures the dynamics is Markovian [32, 51]. It is important to notice that this sequence is only valid for a pure dephasing dynamics, since for more involved interactions including energy exchange the contributions of Ω and Δ in the rates are mixed.

In a recent work [52], the authors showed that there are some particular cases where an oscillation in Coherence leads to a false positive when detecting NM with $\mathcal{N}_C$ in Eq. (3). This scenario can be achieved for other orbital states of color centers, for instance, for the ground state dynamics of the silicon-vacancy center in diamond. We observed that for a phonon super-Ohmic SDF describing energy exchange, the secular approximation has an important role on this false positive with $\mathcal{N}_C$ [53]. In what follows, we show that the approximations considered along this manuscript for optical orbital states are well satisfied. Firstly, we considered only a single ground state $|g\rangle$ and a single electronically excited state $|e\rangle$ with an energy gap $\hbar\omega_{eg} = 1.68$ eV [54] (SiV^-) and $\hbar\omega_{eg} = 1.95$ eV (NV^-) [41]. Phonons will not be able to trigger the $|g\rangle \leftrightarrow |e\rangle$ transition given that the highest phonon energy only reaches 160 meV [55]. Hence, in the absence of this transition we can describe the orbital-phonon dynamics using the pure dephasing model. Secondly, the secular approximation is extensively used and valid for color centers [44]. To support this, we can look at the time scale defined by $T_s = |\omega - \omega'|^{-1}$. If T_s is much smaller than the dissipation time scale τ, the terms with $\omega \neq \omega'$ lead to a vanishing contribution in the dynamics [56]. Such is the case for the ground and excited states of color centers since $T_s \sim \omega_{eg}^{-1} \sim 1$ fs $\ll \tau$, where $\tau \sim 1$ ps is the typical dissipation time scale for phonons.

B. Coherent maps in the strong-coupling regime

Beyond the weak coupling regime the generalized polaron transformation offers the possibility to apply a similar procedure for strong system-bath interactions [57, 58]. This transformation is defined as $H' = e^{S_1} H e^{-S_1}$ with $S_1 = \sigma_z \sum_k (f_k/\omega_k)(b_k^\dagger - b_k)$ and leads to $H' = H_s + H_{ph} + V$, where $H_s = (\Delta/2)\sigma_z + (\Omega_R/2)\sigma_x$ is the system Hamiltonian (neglecting the polaron shift), $H_{ph} = \sum_k \omega_k b_k^\dagger b_k$ is the phonon Hamiltonian, $V = \sigma_x V_x + \sigma_y V_y + \sigma_z V_z$ is the interaction Hamiltonian (see Eqs. (F3)-(F5)) and $\Omega_R = B\Omega$, where B is the renormalization factor [57, 58], see Appendix F. In Figure 3-(d) we plotted the renormalization factor B for the full polaron transformation (FPT) ($f_k = g_k$) and the variational polaron transformation (VPT) ($f_k = F(\omega_k)g_k$), where $F(\omega_k) = [1 + \Omega_R^2/(\omega_k\omega_0)\coth(\beta\omega_k/2)\tanh(\beta\omega_0/2)]^{-1}$. We observed that for not too large values of Ω, the renormalized term $(\Omega_R/2)\sigma_x$ has a negligible effect in the open dynamics above a temperature $T \approx 120$ K. This temperature is very close to the temperature associated with the quasi-localized phonon mode $T_{loc} = \hbar\omega_{loc}/k_B \approx 116$ K. Therefore, oscillations induced by σ_x on the coherence will not be observed at high temperatures [57].

VI. CONCLUSIONS

In summary, we studied the dynamics of SiV^- and NV^- centers due to the vibrations of the diamond lattice and found that the competition of acoustic and quasi-localized phonon modes give rise to a NM dynamics with a rich thermal dependence. As a consequence, different measures of non-Markovianity (NM) exhibit opposite dependence at high temperature, suggesting that the power of each measure will rely on how it is linked to a specific application. In addition, we focus on a simple measure based on Coherence to quantify the degree of NM that takes advantage of the pure dephasing dynamics and measures the back-flow of information from the environment to the system. We compare it with other established measures of NM [9, 11, 31], and observed that it is well-behaved both at low and high temperatures. Also, it is easy to compute and experimentally accessible through Ramsey spectroscopy, which make it suitable for quantifying NM in color centers in diamond [43]. Furthermore, for coherent dynamical maps (general spin-boson model) and a pure dephasing interaction with phonons, this NM measure can be used in the weak coupling limit to identify whether the NM signature solely comes from the reservoir, by following a specific experimental sequence where one can filter out the contribution of the σ_x-term. Even more, for the strong coupling regime we found a temperature $T \approx 120$ K above which this term is negligible.

VII. ACKNOWLEDGMENTS

We are grateful to Felipe Fanchini and Martin Plenio for fruitful discussions about non-Markovianity. AN acknowledges financial support from Universidad Mayor through the Postdoctoral fellowship. JRM acknowledges support from Fondecyt Regular No. 1180673 and AFOSR FA9550-18-1-0513. PR acknowledges support from the Austrian Science Fund (FWF) through Grant No. P32299-N27. RC

acknowledge financial support from Fondecyt Iniciación No. 11180143.

Appendix A: Master Equation

For an interaction Hamiltonian of the form $H_I = (\sigma_z/2)\sum_k g_k(a_k + a_k^\dagger) + (\sigma_x/2)\sum_k \lambda_k(a_k + a_k^\dagger)$ the master equation can be written as

$$\dot{\rho} = -i\left[\frac{1}{2}\omega_0 S_z, \rho\right] + \sum_{i=z,\pm}\frac{\gamma_i(t)}{2}\left[S_i\rho S_i^\dagger - \frac{1}{2}\{S_i^\dagger S_i, \rho\}\right], \tag{A1}$$

where we have neglected the Lamb-shift according our numerical simulations and we have performed the secular approximation. The time-dependent decay rates are defined as

$$\gamma_z(t) = \left(\frac{\Delta}{\omega_0}\right)^2\gamma_1^0(t) + \left(\frac{\Omega}{\omega_0}\right)^2\gamma_2^0(t) + 2\frac{\Omega\Delta}{\omega_0^2}\gamma_3^0(t) \tag{A2}$$

$$\gamma_\pm(t) = \left(\frac{\Omega}{\omega_0}\right)^2\gamma_1^\pm(t) + \left(\frac{\Delta}{\omega_0}\right)^2\gamma_2^\pm(t) - 2\frac{\Omega\Delta}{\omega_0^2}\gamma_3^\pm(t) \tag{A3}$$

The functions $\gamma_i^\eta(t)$ $(i = 1, 2, 3,\ \eta = 0, +, -)$ are given by

$$\gamma_i^\eta(t) = \int_0^\infty J_i(\omega)\left[n(\omega)\frac{\sin(\omega - \eta\omega_0)t}{\omega - \eta\omega_0} + [n(\omega)+1]\frac{\sin(\omega + \eta\omega_0)t}{\omega + \eta\omega_0}\right]d\omega, \tag{A4}$$

where $n(\omega) = [\exp(\hbar\omega/k_BT) - 1]^{-1}$ is the mean number of phonons at thermal equilibrium, k_B is the Boltzmann constant, and T is the reservoir temperature. The spectral density functions are defined as

$$J_1(\omega) = \sum_k |g_k|^2\delta(\omega - \omega_k), \quad J_2(\omega) = \sum_k |\lambda_k|^2\delta(\omega - \omega_k). \tag{A5}$$

The third spectral density function is given by $J_3(\omega) = \sum_k g_k\lambda_k\delta(\omega - \omega_k)$, if the couplings are real. In this case it is straightforward to show that $J_3(\omega) = \sqrt{J_1(\omega)J_2(\omega)}$. For $J_2(\omega) = 0$ (no energy-exchange) also $J_3(\omega) = 0$ and we obtain

$$\dot{\rho}_{ee} = \frac{1}{2}\gamma_+(t) - \frac{1}{2}\left(\gamma_+(t) + \gamma_-(t)\right)\rho_{ee}, \tag{A6}$$

$$\dot{\rho}_{eg} = -i\omega_0\rho_{eg} - \left[\gamma_z(t) + \frac{1}{4}\left(\gamma_+(t) + \gamma_-(t)\right)\right]\rho_{eg}, \tag{A7}$$

where $\rho_{ee}(t) = \langle e_+|\rho(t)|e_+\rangle$, $\rho_{gg}(t) = \langle e_-|\rho(t)|e_-\rangle$ and $\rho_{eg}(t) = \langle e_+|\rho(t)|e_-\rangle$. The above equations can be formally integrated,

$$\rho_{ee}(t) = \rho_{ee}(0)e^{F(t)} + e^{F(t)}\int_0^t g(t_1)e^{-F(t_1)}\,dt_1, \tag{A8}$$

$$\rho_{eg}(t) = \rho_{eg}(0)e^{-i\omega_0 t - F_0(t)}e^{F(t)/2}, \tag{A9}$$

where $F(t) = -(1/2)\int_0^t(\gamma_+(t_1) + \gamma_-(t_1))\,dt_1$, $g(t) = \gamma_+(t)/2$, and $F_0(t) = \int_0^t\gamma_z(t_1)\,dt_1$. Notice that $F_0(t)$ corresponds to the dynamics induced by S_z, which does not generate coherence. Only the contribution of $F(t)$ in Eq. (A9) will lead to non-Markovianity, and therefore we will cancel it. To do so, we first calculate the expectation values of S_z for different initial conditions.

$$\langle S_z\rangle_{(\rho_{ee}=1)} = 2e^{F(t)} + \langle S_z\rangle_{(\rho_{ee}=1)}, \tag{A10}$$

$$\langle S_z\rangle_{(\rho_{gg}=1)} = 2e^{F(t)}\int_0^t g(t_1)e^{-F(t_1)}\,dt_1 - 1. \tag{A11}$$

From these results it is straight forward to show that

$$S = \frac{\langle S_z\rangle|_{\rho(0)=|e\rangle\langle e|} - \langle S_z\rangle|_{\rho(0)=|g\rangle\langle g|}}{2} = e^{F(t)}, \tag{A12}$$

Furthermore, the renormalized Coherence is defined as $\tilde{C}(t) = C(t)\times S^{-1/2} = 2\rho_{eg}(0)e^{-F_0(t)}$, where for an incoherent dynamics $S = 1$. Finally, one can observe that this expression for the Coherence has no contribution from $(\Omega/2)\sigma_x$ in Eq. (4) (as opposed to the case where $C(t)$ is calculated directly from Eq. (A9) and even more, we have not done any assumption about the spectral density function $J(\omega)$, which makes this approach quite general.

Appendix B: Dephasing rate induced by strong interactions with quasi-localized phonons

The dephasing rate associated with the strong interaction with a quasi-localized phonon mode is given by

$$\gamma_{loc1}(t) = \frac{J_0\Gamma}{2}\int_0^\infty \frac{\omega^2\coth\left(\frac{\omega}{2k_BT}\right)\sin(\omega t)}{\left(\frac{\omega}{\omega_{loc}}+1\right)^2(\omega-\omega_{loc})^2 + (\Gamma/2)^2}\,d\omega. \tag{B1}$$

This integral can be solved analytically, however, we show next a method to obtain a good approximation that gives us a better understanding of the effect of the width Γ, the frequency of the quasi-localized phonon ω_{loc}, the amplitude J_0, and temperature T. Using the change of variable $u = \omega - \omega_{loc}$ and extending the lower limit of the integration to $-\infty$ (assuming $\omega_{loc} \gg 1$), we obtain

$$\gamma_{loc1}(t) \approx J_0\cos(\omega_{loc}t)\int_{-\infty}^\infty f(u)\sin(ut)\,du + J_0\sin(\omega_{loc}t)\int_{-\infty}^\infty f(u)\cos(ut)\,du, \tag{B2}$$

where

$$f(u) = \frac{(u+\omega_{loc})^2\coth\left(\frac{u+\omega_{loc}}{2k_BT}\right)}{(u/\omega_{loc}+2)^2}\frac{\Gamma/2}{u^2+(\Gamma/2)^2}. \tag{B3}$$

The main contribution in both integrals given in Eq. (B2) comes from the narrow Lorentzian function $L(u) = (\Gamma/2)/(u^2 + (\Gamma/2)^2)$ centered around the value $u = 0$ (main

peak around $\omega = \omega_{loc}$ for $J(\omega)$, see Figure 1). Using the approximation

$$f(u) \approx \frac{1}{4}\omega_{loc}^2 \coth\left(\frac{\omega_{loc}}{2k_BT}\right)\frac{\Gamma/2}{u^2+(\Gamma/2)^2}, \quad \text{(B4)}$$

and the symmetry consideration $\int_{-\infty}^{\infty} f(u)\sin(ut)\,du = 0$, we obtain

$$\gamma_{loc1}(t) \approx \frac{\pi J_0 \omega_{loc}^2}{4}\coth\left(\frac{\omega_{loc}}{2k_BT}\right)\sin(\omega_{loc}t)e^{-\Gamma t/2}, \quad \text{(B5)}$$

which corresponds to a damped periodic oscillation, where ω_{loc} is the frequency, $\Gamma/2$ is the decay rate and both temperature T and strength J_0 determine the maximum amplitude of the oscillations. At zero temperature, $\coth(\hbar\omega/2k_BT) = 1$, and therefore, we recover the expression given in Eq. (13). At high temperatures, $k_BT \gg \hbar\omega_{loc}$, we have $\coth(\hbar\omega/2k_BT) \approx 2k_BT/\hbar\omega$, and then

$$\gamma^{\uparrow}_{loc1}(t) \approx \left(\frac{2k_BT}{\omega_{loc}}\right)\gamma^{\downarrow}_{loc1}(t). \quad \text{(B6)}$$

Appendix C: Dephasing Rate for an NV$^-$ center

The dephasing rate $\gamma_{NV}(t)$ is plotted in Figure 4, calculated from Eq. (6) with the spectral density function given numerically in Ref. [41] and illustrated in Figure 1.

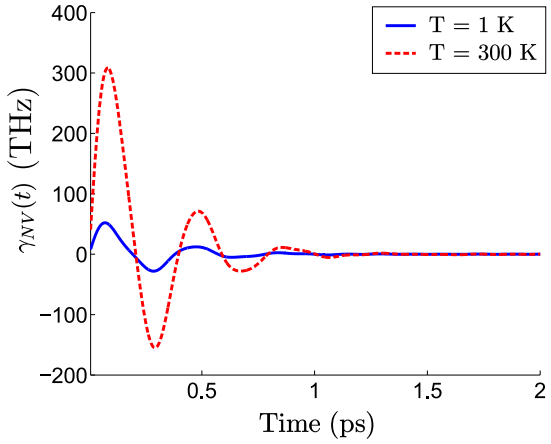

FIG. 4. Dephasing rate for the NV$^-$ center in diamond for temperatures $T = 1$ K and $T = 300$ K. The period of the oscillations are given approximately by $2\pi/\omega \approx 0.4$ ps, where $\omega = 15.7$ THz is the frequency of the main peak of the spectral density function of the NV$^-$ center.

Appendix D: Role of different spectral density function on the Coherence

From Figure 3-(b), it is easy to see that Coherence $C(t)$ obeys two different regimes separated in temperature. At low temperature, the time evolution of $C(t)$ has contributions from of all the spectral density functions in Eqs. (9)-(11), however the strong oscillation in the main plot evidences that γ_{loc1} has the leading contribution. Even when one would expect γ_{loc1} to hold as the leading term in the dynamics at high temperatures, see Figure 2, this is not the case. In Figure 5 we show $C(t)$ for two particular decay rates, namely $\gamma_{bulk}(t)$ (solid) and $\gamma_{loc1}(t)$ (dashed), at 300 K. It is remarkable that $\gamma_{bulk}(t)$ reproduces the behavior (in terms of Non-Markovianity) depicted in the inset of Figure 3-(b), despite that it decays slower due to the absence of the other decay rates. This outcome supports the statement that only bulk phonons are relevant at high temperature [47, 48]. In contrast, $\gamma_{loc1}(t)$ shows a very interesting dynamics as well.

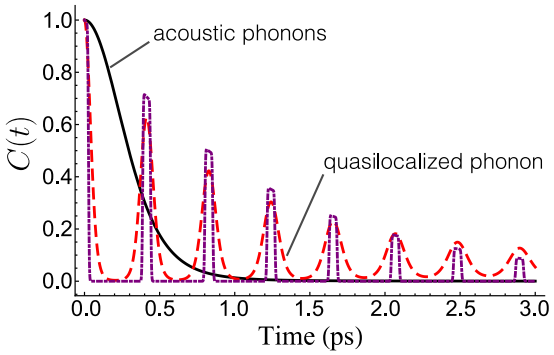

FIG. 5. Behavior of the coherence function $C(t)$ at $T = 300$ K. Solid line (evaluated for $J_{bulk}(\omega)$ only) evidences that bulk phonons have the main contribution to the dynamics. Moreover, dashed line (evaluated for $J_{loc1}(\omega)$ only), evidences that quasilocalized phonon modes can be roughly reproduced with an interaction with a coherent state and a phenomenological decay (dot-dashed).

In particular, similar behavior have been observed in spin-echo spectroscopy for a single NV$^-$ [59] or an ensemble [60] interacting with a natural environment of ^{13}C nuclear spins, where the collapses and revivals originate from a coherent interaction with individual proximal nuclear spins, and the revivals decay comes from the interaction with the ^{13}C bath. In the same way, this behavior has been observed for a single NV interacting with a mechanical oscillator [61]. In agreement with these results, we suggest that the interaction with this quasi-localized phonon mode can be though as an interaction with a single mode in a coherent state, with an added phenomenological decay that goes as $\exp(-\Gamma t)$, being $\Gamma = 0.8414$ THz the width of the Lorentzian spectral density function. The composite state after this interaction is given by [62],

$$|\Psi\rangle = (|e\rangle|\beta_{\uparrow}\rangle + e^{-2i\lambda\beta\sin(t\omega_{loc})}|g\rangle|\beta_{\downarrow}\rangle)/\sqrt{2}, \quad \text{(D1)}$$

where $\xi = 1 - e^{-it\omega_{loc}}$, $|\beta_{\uparrow}\rangle = |\beta e^{-it\omega_{loc}} + \lambda\xi\rangle$ ($|\beta_{\downarrow}\rangle = |\beta e^{-it\omega_{loc}} - \lambda\xi\rangle$) is the displaced coherent state, $\lambda = (\int_0^{\infty} J_{loc1}(\omega))^{1/2}\,d\omega$. Even more, we approximated $|\beta|^2$ to the thermal occupancy phonon number $n(\omega_{loc}) = [\exp(\hbar\omega_{loc}/k_bT) - 1]^{-1}$, given that at $T = 300$ K the occupancy is small ($n(\omega_{loc}) \approx 2$). Finally, after tracing out

over the coherent state degrees of freedom we are able to calculate $C(t)$. This highly simplified model is capable to capture the collapses, revivals, and the overall decay, as illustrate by the dot-dashed curve.

Appendix E: Measures of the degree of non-Markovianity

For comparison, we introduce now the Breuer-Laine-Piilo (BLP) measure [9], which is based on the trace distance

$$\mathcal{N}_{BLP} = \max_{\rho_{1,2}(0)} \int_{dD/d\tau>0} \frac{dD(\rho_1,\rho_2)}{d\tau}\, d\tau, \qquad \text{(E1)}$$

where $D(\rho_1,\rho_2) = \mathrm{Tr}|\rho_1(t)-\rho_2(t)|/2$ and $|A| = \sqrt{A^\dagger A}$. For the spin-boson model ($\Omega = 0$ in Eq. (4)), the maximization can be exactly solved and one obtains [63]

$$\mathcal{N}_{BLP} = -2\int_{\gamma(t)<0} \gamma(t)|b|^2 e^{-\Gamma(t)}(a^2+|b|^2e^{-\Gamma(t)})^{-1/2}, \qquad \text{(E2)}$$

where $a = \langle e|(\rho_1(0)-\rho_2(0))|e\rangle$, $b = \langle e|(\rho_1(0)-\rho_2(0))|g\rangle$, $\gamma(t)$ is given in Eq. (6), and $\Gamma(t) = 2\int_0^t \gamma(\tau)\, d\tau$.

The BLP measure is plotted in Figure. 6 (dotted line) for the initial states

$$\rho_1(0) = \frac{1}{2}\begin{pmatrix} 1 & 1 \\ 1 & 1 \end{pmatrix}, \qquad \rho_2(0) = \frac{1}{2}\begin{pmatrix} 1 & -1 \\ -1 & 1 \end{pmatrix}. \qquad \text{(E3)}$$

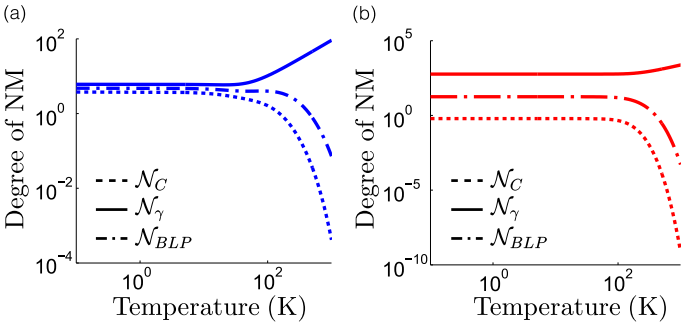

FIG. 6. Comparison between different measures of non-Markovianity as a function of temperature for the (a) SiV^- center, and (b) NV^- center in diamond using $\Omega = 0$ and $\Delta = 1$.

Notice that $\mathcal{N}_\gamma$ (solid line) shows a thermal dependence that is based on the dephasing rate $\gamma(t)$ given in Eq. (6), and it has a strictly increasing behavior leading to a large degree of NM when the temperature is above some critical value $T \sim 30$ K. However, we observed that $\mathcal{N}_{BLP}$ shows a strictly decreasing behavior leading to a small degree of NM at room temperature. Finally, $\mathcal{N}_C$ (dashed-line) shows a thermal dependence that is similar to $\mathcal{N}_{BLP}$, as one would expect since both NM measures are based on the back-flow of quantum information.

Appendix F: Strong coupling model

In order to study strong interactions between a two-level system and its phononic environment we introduce the following general polaron transformation [57, 58] ($\hbar = 1$)

$$H' = e^{S_1} H e^{-S_1}, \qquad S_1 = \sigma_z \sum_k \frac{f_k}{\omega_k}(b_k^\dagger - b_k), \qquad \text{(F1)}$$

where $f_k = g_k$ corresponds to the the full polaron transformation (FPT). If we apply the above transformation on the general spin-boson Hamiltonian $H = (\Delta/2)\sigma_z + (\Omega/2)\sigma_x + \sum_k \omega_k b_k^\dagger b_k + \sigma_z \sum_k g_k(b_k^\dagger + b_k)$, we obtain

$$H' = \frac{\Delta}{2}\sigma_z + \frac{\Omega_R}{2}\sigma_x + \sum_k \frac{f_k}{\omega_k}(f_k - 2g_k) + \sum_k \omega_k b_k^\dagger b_k + V. \qquad \text{(F2)}$$

The interaction Hamiltonian is given by $V = \sigma_x V_x + \sigma_y V_y + \sigma_z V_z$, where

$$V_x = \frac{\Omega}{4}(B_+ + B_- - 2B), \qquad \text{(F3)}$$

$$V_y = \frac{\Omega}{4i}(B_- - B_+), \qquad \text{(F4)}$$

$$V_z = \sum_k (g_k - f_k)(b_k^\dagger + b_k). \qquad \text{(F5)}$$

The bath operators are defined as

$$B_\pm = \exp\left[\pm 2\sum_k \frac{f_k}{\omega_k}(b_k^\dagger - b_k)\right], \qquad \text{(F6)}$$

$$B = \langle B_\pm\rangle_{ph} = \exp\left[-2\sum_k \frac{f_k^2}{\omega_k^2}\coth\left(\frac{\beta\omega_k}{2}\right)\right], \qquad \text{(F7)}$$

with $\beta = (k_B T)^{-1}$ and the expectation value is calculated using the thermal phonon state $\rho_{ph} = \exp(-\beta H_{ph})/\mathrm{Tr}\{\exp(-\beta H_{ph})\}$. To determine the optimal values of f_k for the variational polaron transformation (VPT) it is necessary to minimize the free energy

$$A_B = -\frac{1}{\beta}\ln \mathrm{Tr}_{A+B}\{e^{-\beta H_0}\} + \langle V\rangle_{H_0}, \qquad \text{(F8)}$$

where $H_0 = H_A + H_B$ is the non-interacting Hamiltonian with $H_A = (\Delta/2)\sigma_z + (\Omega_R/2)\sigma_x + \sum_k (f_k/\omega_k)(f_k - 2g_k)$ and $H_B = \sum_k \omega_k b_k^\dagger b_k$. Using $\langle V\rangle_{H_0} = 0$ and the condition $dA_B/df_k = 0$ we obtain that $f_k = g_k F(\omega_k)$, where

$$F(\omega_k) = \left[1 + \frac{\Omega_R^2}{\omega_k\omega_0}\coth\left(\frac{\beta\omega_k}{2}\right)\tanh\left(\frac{\beta\omega_0}{2}\right)\right]^{-1}, \qquad \text{(F9)}$$

$$\Omega_R = \Omega B, \qquad \text{(F10)}$$

and $\omega_0 = \sqrt{\Delta^2 + \Omega_R^2}$. In the continuum limit, the renormalization factor B is given by

$$B = \exp\left[-2\int_0^\infty \frac{J(\omega)}{\omega^2}F^2(\omega)\coth\left(\frac{\beta\omega}{2}\right)\, d\omega\right]. \qquad \text{(F11)}$$

This renormalization factor depends on the shape of the SDF $J(\omega) = \sum_k |g_k|^2\delta(\omega - \omega_k)$, the reservoir temperature T, and must be calculated from self-consistency between Eqs. (F9)-(F11).

[1] M. A. Nielsen and I. L. Chuang, Quantum Computation and Quantum Information (Cambridge Univ. Press, Cambridge, UK, 2000).

[2] V. Giovannetti, S. Lloyd, and L. Maccone, Science **306**, 1330 (2004).

[3] C. Gross, T. Zibold, E. Nicklas, J. Estève, and M. K. Oberthaler, Nature **464**, 1165 (2010).

[4] H. Breuer and F. Petruccione, The Theory of Open Quantum Systems (Oxford University Press, Oxford, 2002).

[5] A. W. Chin, S. F. Huelga, M. B. Plenio, Phys. Rev. Lett. **109**, 233601 (2012).

[6] B. Bylicka, D. Chruściński and S. Maniscalco, Sc. Rep. **4**, 5720 (2014).

[7] N. Mirkin, P. Poggi, and D. Wisniacki, Phys. Rev. A **99**, 020301(R) (2019).

[8] D. M. Reich, N. Katz, and C. P. Koch, Sc. Rep. **5**, 12430 (2015).

[9] H.-P. Breuer, E.-M. Laine, and J. Piilo, Phys. Rev. Lett. **103**, 210401 (2009); E.-M. Laine, J. Piilo, and H.-P. Breuer, Phys. Rev. A **81**, 062115 (2010).

[10] S. Luo, S. Fu, and H. Song, Phys. Rev. A **86**, 044101 (2012).

[11] A. Rivas, S. F. Huelga, and M. B. Plenio, Phys. Rev. Lett. **105**, 050403 (2010); A. Rivas, S. F. Huelga, and M. B. Plenio, Rep. Prog. Phys. **77**, 094001 (2014).

[12] D. Chruściński and S. Maniscalco, Phys. Rev. Lett. **112**, 120404 (2014).

[13] T. Chanda, S. Bhattacharya, Ann. Phys. **366**, 1 (2016).

[14] M. H. M. Passos, P. C. Obando, W. F. Balthazar, F. M. Paula, J. A. O. Huguenin, and M. S. Sarandy, arXiv:1807.05378 (2018).

[15] A. Gruber, A. Drabenstedt, C. Tietz, L. Fleury, J. Wrachtrup, and C. von Borczyskowski, Science **276**, 2012 (1997).

[16] E. van Oort, N. B. Manson, and M. Glasbeek, J. Phys. C, **21**, 4385 (1988).

[17] J. N. Becker, B. Pingault, D. Gross, M. Gündogan, N. Kukharchyk, M. Markham, A. Edmonds, M. Atatüre, P. Bushev, and C. Becher, Phys. Rev. Lett. **120**, 053603 (2018).

[18] J. R. Maze, P. L. Stanwix, J. S. Hodges, S. Hong, J. M. Taylor, P. Cappellaro, L. Jiang, M. V. Gurudev Dutt, E. Togan, A. S. Zibrov, A. Yacoby, R. L. Walsworth, and M. D. Lukin, Nature **445**, 644 (2008).

[19] M. V. Gurudev Dutt, L. Childress, L. Jiang, E. Togan, J. Maze, F. Jelezco, A. S. Zibrov, P. R. Hemmer, and M. D. Lukin, Science **316**, 1321 (2007).

[20] A. J. Leggett, S. Chakravarty, A. T. Dorsey, Matthew P. A. Fisher, Anupam Garg, and W. Zwerger Rev. Mod. Phys. 59, 1 (1987).

[21] K. V. Kepesidis, M.-A. Lemonde, A. Norambuena, J. R. Maze, and P. Rabl, Phys. Rev. B **94**, 214115 (2016).

[22] M. Abdi and M. B. Plenio, Phys. Rev. Lett. **122**, 023602 (2019).

[23] M.-A. Lemonde, S. Meesala, A. Sipahigil, M. J. A. Schuetz, M. D. Lukin, M. Loncar, and P. Rabl, Phys. Rev. Lett. **120**, 213603 (2018).

[24] M. C. Kuzyk and H. Wang, Phys. Rev. X **8**, 041027 (2018).

[25] P.-Bo Li, X.-Xiao Li, F. Nori, arXiv:1901.04650.

[26] Z.-X. Man, Y.-J. Xia, and R. Lo Franco, Phys. Rev. A **97**, 062104 (2018).

[27] A. Rivas, Phys. Rev. A **95**, 042104 (2017).

[28] T. Baumgratz, M. Cramer, and M. B. Plenio, Phys. Rev. Lett. **113**, 140401 (2014).

[29] Note that $\mathcal{N}_C$ may fail in the presence of non secular terms or longitudinal relaxation.

[30] A. Streltsov, G. Adesso, and M. B. Plenio, Rev. Mod. Phys. **89**, 041003 (2017).

[31] M. J. W. Hall, J. D. Cresser, L. Li and E. Andersson, Phys. Rev. A **89**, 042120 (2014).

[32] P. Haikka, T. H. Johnson, and S. Maniscalco, Phys. Rev. A **87**, 010103(R) (2013).

[33] B. Vacchini, A. Smirne, E.-M. Laine, J. Piilo, and H.-P. Breuer, New J. Phys. **13**, 093004 (2011).

[34] A. Leggett, S. Chakravarty, A. Dorsey, M. Fisher, A. Garg, and W. Zwerger, Rev. Mod. Phys. **59**, 1 (1987).

[35] U. Weiss, *Quantum Dissipative Systems*, vol. 3rd ed. (World Scientific, Singapore, 2008).

[36] A. Norambuena, S. A. Reyes, J. Mejía-López, A. Gali, and J. R. Maze, Phys. Rev. B **94**, 134305 (2016).

[37] J. Luczka, Physica A **167**, 919 (1990).

[38] A. Dietrich, K. D. Jahnke, J. M. Binder, T. Teraji, J. Isoya, L. J. Rogers, and F. Jelezko, New. J. Phys. **16**, 113019 (2014).

[39] E. Londero, G. Thiering, L. Razinkovas, A. Gali, and A. Alkauskas, Phys. Rev. B **98**, 035306 (2018).

[40] G. Thiering and A. Gali, Phys. Rev. X **8**, 021063 (2018).

[41] A. Alkauskas, B. B. Buckley, D. D. Awschalom, and C. G. Van de Walle, New J. Phys. **16**, 073024 (2014).

[42] R. Ulbricht, S. Dong, A. Gali, S. Meng, and Z.-Heng Loh, Phys. Rev. B 97, 220302(R) (2018).

[43] J. F. Haase, P. J. Vetter, T. Unden, A. Smirne, J. Rosskopf, B. Naydenov, A. Stacey, F. Jelezko, M. B. Plenio, and, S. F. Huelga, Phys. Rev. Lett. **121**, 060401 (2018).

[44] A. Norambuena, E. Muñoz, H. T. Dinani, A. Jarmola, P. Maletinsky, D. Budker, and J. R. Maze, Phys. Rev. B **97**, 094304 (2018).

[45] R. Betzholz, J. M. Torres, and M. Bienert, Phys. Rev. A **90**, 063818 (2014).

[46] R. Vasile, F. Galve, and R. Zambrini, Phys. Rev. A **89**, 022109 (2014).

[47] M.L. Goldman, A. Sipahigil, M.W. Doherty, N.Y. Yao, S.D. Bennett, M. Markham, D.J. Twitchen, N.B. Manson, A. Kubanek, and M.D. Lukin, Phys. Rev. Lett. **114**, 145502 (2015).

[48] M. L. Goldman, M. W. Doherty, A. Sipahigil, N. Y. Yao, S. D. Bennett, N. B. Manson, A. Kubanek, and M. D. Lukin, Phys. Rev. B **91**, 165201 (2015).

[49] G. Guarnieri, A. Smirne, and B. Vacchini, Phys. Rev. A **90**, 022110 (2014).

[50] E-M Laine, Phys. Scr. **T140**, 014053 (2010).

[51] F. F. Fanchini, L. K. Castelano, and A. O. Caldeira, New. J. Phys. **12**, 073009 (2010).

[52] J. F. Haase, A. Smirne, and S. F. Huelga, arXiv:1903.11118 (2019).

[53] This work is in preparation and the results will be given elsewhere.

[54] T. Feng and B. D. Schwartz, Journal of Applied Physics 73, 1415 (1993).

[55] P. Pavone, K. Karch, O. Schutt, W. Windl, D. Strauch, P. Giannozzi, and S. Baroni, Phys. Rev. B 48, 3156 (1993).

[56] I. Vega and D. Alonso, Rev. Mod. Phys. **89**, 015001 (2017).

[57] K. Agarwal, I. Martin, M. D. Lukin, and E. Demler, Phys. Rev. B **87**, 144201 (2013).
[58] D. P. S. McCutcheon and A. Nazir, Phys. Rev. B **83**, 165101 (2011).
[59] L. Childress, M. V. Gurudev Dutt, J. M. Taylor, A. S. Zibrov, F. Jelezko, J. Wrachtrup, P. R. Hemmer, M. D. Lukin, Science **314**, 281 (2006).
[60] P. L. Stanwix, L. M. Pham, J. R. Maze, D. Le Sage, T. K. Yeung, P. Cappellaro, P. R. Hemmer, A. Yacoby, M. D. Lukin, and R. L. Walsworth, Phys. Rev. B **82**, 201201(R) (2010).
[61] S. D. Bennet, S. Kolkowitz, Q. P. Unterreithmeier, P. Rabl, A. C. Bleszynski, J. G. Harris, and M. D. Lukin, New. J. Phys. **14**, 125004 (2012).
[62] V. Montenegro, R. Coto, V. Eremeev, and M. Orszag, Phys. Rev. A **98**, 053837 (2018).
[63] H.-Sheng Zeng, N. Tang, Y.-Ping Zheng, and G.-You Wang, Phys. Rev. A **84**, 032118 (2011).